INTERNATIONAL JOURNAL OF CLIMATOLOGY
Int. J. Climatol. **29**: 2146–2155 (2009)
Published online 8 January 2009 in Wiley InterScience
(www.interscience.wiley.com) DOI: 10.1002/joc.1845

RMetS
Royal Meteorological Society

Statistical-dynamical prediction of the Madden–Julian oscillation using NCEP Climate Forecast System (CFS)

Kyong-Hwan Seo*
Division of Earth Environmental System, Pusan National University, Busan, Korea

ABSTRACT: The predictive performance of the Madden–Julian Oscillation (MJO) in the National Centers for Environmental Prediction's (NCEP's) operational coupled, Climate Forecast System (CFS) model is assessed and statistical-dynamical hybrid models are developed based on this numerical model to improve forecasting skill. By projecting ENSO-removed variables onto the principal patterns of the MJO convection and upper- and lower-level circulations, MJO-related signals in the dynamical model forecasts are extracted. It is found that the coupled model exhibits useful predictability out to 2 and 3 pentads when the initial MJO convection is located over the Maritime Continent and the Indian Ocean, respectively. The first hybrid model (HYBRID1) developed is a lagged multiple linear regression scheme, where the previous values of the first two leading principal components (PCs) from the coupled model are used as predictors along with the latest observed PC values. The other hybrid model (HYBRID2) is constructed to fit the predicted PC time series from the coupled model to the observed PCs at each lead time using 13 years of training data fields. HYBRID2 does not produce persistent improvement in forecast skill compared to CFS, whereas for HYBRID1, the resulting correlation coefficient and root mean square (RMS) skills are considerably enhanced due to the incorporation of lagged correlation information between the two PCs. The skill improvement of HYBRID1 ranges from 15 to 50% relative to the CFS forecast and the improvement in the correlation skill is greater than the RMS error correction. When the MJO convection is located initially over the Maritime Continent during the northern summer, the CFS forecast skill is as small as the persistence forecast, whereas HYBRID1 demonstrates the greatest skill improvement. During ENSO winters, the forecast skill is enhanced by ∼30% by HYBRID1. In particular, the skill improvement in La Niña years is noticeably greater than in El Niño years.

KEY WORDS Madden–Julian oscillation (MJO); coupled CFS model; statistical-dynamical hybrid model; predictive skill

Received 4 December 2007; Revised 17 November 2008; Accepted 2 December 2008

1. Introduction

The Madden–Julian Oscillation (MJO) is the most dominant mode of tropical intraseasonal variability in the atmosphere (Madden and Julian, 1971, 1972). The MJO affects global weather and climate through teleconnections (e.g. Trenberth *et al*., 1998; Higgins *et al*., 2000; Jeong *et al*., 2008). The MJO also interacts with the monsoon systems over Asia, Australia, and the Americas (Lau and Chan, 1986; Mo, 2000; Higgins and Shi, 2001; Jones and de Carvalho, 2002; Wheeler and Hendon, 2004, and others) and modulates tropical cyclone activity (e.g. Maloney and Hartmann, 2000; Kim *et al*., 2008 and references therein) and the development of ENSO (McPhaden, 1999, 2004; Kessler and Kleeman, 2000; Zhang and Gottschalck, 2002; Seo and Xue, 2005).

This global influence exerted by the MJO on meteorology and climate necessitates its accurate forecast in numerical models. However, in reality, operational general circulation models (GCMs) have difficulty in forecasting the MJO. In particular, the long-term MJO simulations by either Atmospheric Model Intercomparison Project (AMIP)-type or Coupled Model Intercomparison Project (CMIP)-type setting are also unable to reproduce the major MJO characteristics satisfactorily, for example, the eastward propagation across the Maritime Continent and the significant peak signals in a 30–70 day period band. The recent investigation on the MJO prediction performance using the National Centers for Environmental Prediction (NCEP) operational GCM [Global Forecast System (hereafter GFS)] (Hendon *et al*., 2000; Jones *et al*., 2000; Seo *et al*., 2005) has shown skillful forecast (measured by anomaly correlation greater than 0.6) only extending out to 10 days, which is well below the potential predictability estimated by twin predictability experiments using the NASA GLA GCM in Waliser *et al*. (2003). They showed useful forecast extending out to about 30 days for 200-hPa velocity potential and to 15 days for rainfall anomalies.

* Correspondence to: Dr Kyong-Hwan Seo, Division of Earth Environmental System, Pusan National University, Busan 609-735, Korea.
E-mail: khseo@pusan.ac.kr

Recently, NCEP's atmosphere-ocean coupled Climate Forecast System (CFS hereafter) model produced hindcast daily output for the period 1982–2004. This dataset provides an opportunity to evaluate the MJO forecast skill in the coupled dynamical model. However, extracting the MJO signal in forecast data is not a straightforward task since a conventional bandpass filter cannot be applied directly to forecast data output. To overcome this difficulty, Jones *et al*. (2000) and Seo *et al*. (2005) employed a padding method where the observed data are concatenated to the GCM forecast output in front and then the padded data are filtered by a typical bandpass time filter. One of the caveats associated with this method is to introduce an artificial skill by transferring the observed signal to the forecast data. In this study, the empirical methods developed by Lo and Hendon (2000, hereafter LH00) and Wheeler and Hendon (2004, hereafter WH04) are used to extract the MJO signal in the CFS model forecast data and assess the forecast performance. These methods extract the MJO by projecting the daily anomaly data, whose annual cycle and interannual variability have been removed in the spatial domain in advance, onto a leading pair of empirical orthogonal functions (EOFs) of the combined fields of tropical outgoing longwave radiation (OLR), 850-hPa zonal wind, and 200-hPa zonal wind. This method has been proven effective for the extraction of MJO-related variability in real time and we apply this approach to the CFS data.

In this study, using the methods described in LH00 and WH04, we assess dynamic predictability of the MJO in the atmosphere-ocean coupled model. In particular, statistical-dynamical hybrid schemes based on the coupled model are developed to correct model deficiency. Furthermore, we evaluate the MJO forecast skills in the coupled dynamical model and hybrid schemes for the winter and summer seasons, and for the ENSO warm and cold phases. In Section 2, the coupled model and datasets are presented along with analysis methods. Section 3 summarizes the two statistical-dynamical hybrid models developed in this study. The forecast skill from the coupled and hybrid models for the different convective phases, seasons, and ENSO states is presented in Section 4.

2. NCEP coupled model and methods

2.1. Datasets

The MJO is a coupled system of deep convection and large-scale circulation in the tropics. Therefore, zonal winds at 200 and 850 hPa and OLR as a proxy for deep convection are used to identify the MJO signal. OLR is derived from the Advanced Very High Resolution Radiometer onboard the National Oceanic and Atmospheric Administration (NOAA) polar orbiting satellites (Liebmann and Smith, 1996). The zonal winds are extracted from the NCEP/DOE Reanalysis 2 (R2) (Kanamitsu *et al*., 2002). Both datasets are on a 2.5×2.5 longitude-latitude grid. These datasets contain daily data from 1982 to 2004. Using the data from 1982 to 1994, the EOFs of the combined fields of the three variables are calculated to capture the convectively coupled large-scale circulation signal associated with the MJO.

2.2. The NCEP coupled model forecast

The atmospheric component of the coupled CFS is the 2003 version of the NCEP GFS with 62 spectral waves (T62) in the horizontal and 64 sigma layers in the vertical directions. The Modular Ocean Model V.3 (MOM3) (Pacanowski and Griffies, 1998) of the Geophysical Fluid Dynamics Laboratory (GFDL) is used as an oceanic component. These atmospheric and oceanic models are coupled once per day. Sea ice extent is prescribed with the observed climatology. More detailed description of the CFS model can be found in Wang *et al*. (2005) and Saha *et al*. (2006).

The coupled CFS model hindcasts are made for the period starting from 1982 to 2004. To reduce the computational burden, the CFS integrations are designed to be initialized on 15 different dates: 9–13, 19–23 and the last two days of the current month and the first three days of the following month. Therefore, a cubic spline interpolation is carried out on these discrete forecast data in order to fill the gaps and facilitate the necessary calculations. This is done for each lead time. To remove systematic model bias, climatology is removed from the forecast and verification data, separately. The climatology is calculated by retaining only the annual mean and first three annual harmonics, representing a smooth annual cycle. Then, anomalies are created by removing this smooth annual cycle from the total field for each variable. For the forecast data, this is applied for each lead time and initialization date. In this study, only 45-day forecast data are used. The corresponding atmospheric GFS hindcast data for the corresponding periods are not available.

2.3. Methods of analysis

To extract only the MJO-related signal in the forecast data, we combine the two methods proposed by LH00 and WH04, which extract intraseasonal signals in the spatial domain not in the frequency space. Briefly, the MJO signal is calculated from the projection of interannual variability-removed anomalies onto the characteristic spatial EOF patterns that represent the convectively coupled large-scale MJO variations. The ENSO-related interannual variability is removed in the spatial domain by calculating the OLR and zonal wind components that are linearly related to the first two EOF modes of the Optimally Interpolated SST data (Reynolds *et al*., 2002). Then, the characteristic spatial EOF patterns are prepared from the EOF analysis of the combined fields of the observed OLR, and 850-hPa and 200-hPa zonal winds averaged over (15 °S, 15°N) for the 1982–1994 period. Prior to inputting to the covariance matrix, each variable is normalized by its global variance to impose the same amount of weighting among the variables. The horizontal distributions of the two leading EOF modes are shown

DOI: 10.1002/joc

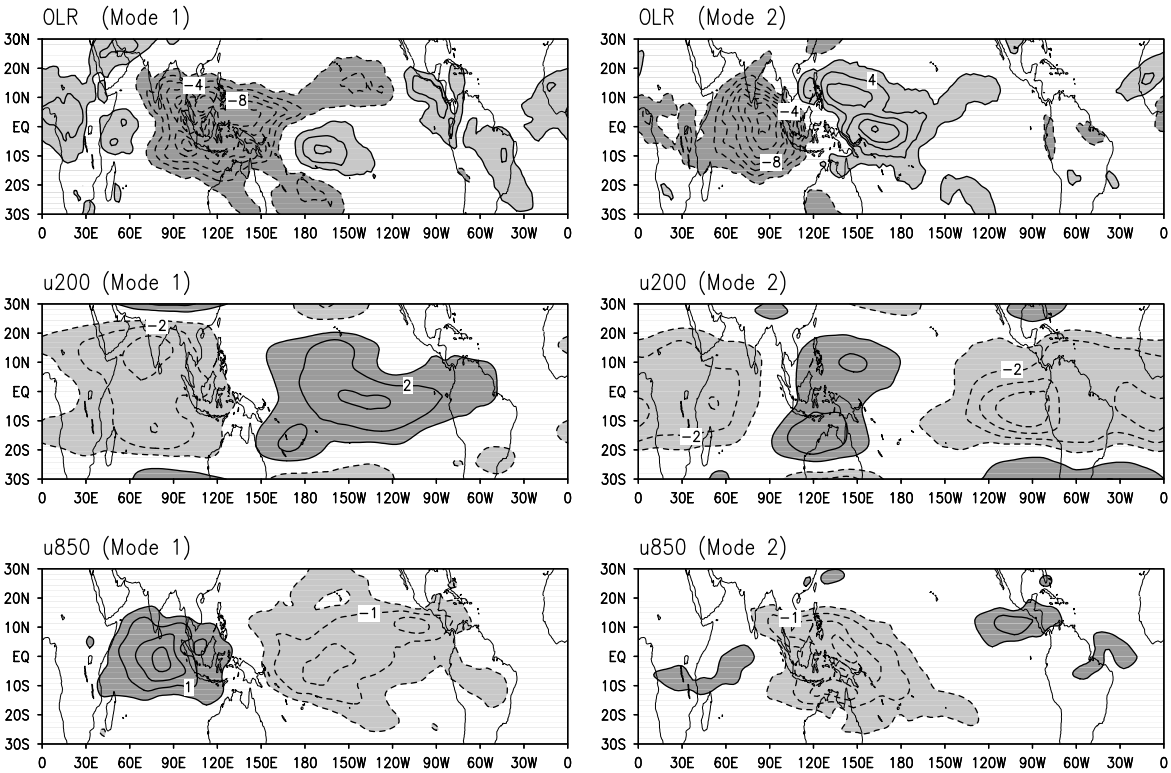

Figure 1. Spatial structures for EOF1 and EOF2 of the combined analysis of interannual-variability-removed OLR, u850 and u200. All variables are normalized by the averaged value of global variance (15.0 W m^{-2} for OLR, 1.9 m s^{-1} for u850, and 4.9 m s^{-1} for u200).

in Figure 1. The first EOF (EOF1; left panels) represents strong convective heating over the Maritime Continent and the western Pacific (100 °E–160 °E), and the convergent flow in the lower troposphere and the divergent flow in the upper troposphere. The second EOF (EOF2; right panels) is characterized by strong deep convection located over the Indian Ocean (60 °E–100 °E). The corresponding large-scale circulation is coherent with the diabatic heating field. The corresponding first two principal component (PC) time series (not shown) represent 12 and 11% of the total variance, respectively. These PCs are significantly correlated with a lag of ~10–12 days, corresponding to a 1/4 period of the MJO. Therefore, these two modes describe the large-scale, eastward-propagating, MJO convection and circulation signal. Composite analysis using the first and second PCs illustrates the evolution of the MJO convection-circulation anomalies during the northern winter and summer (not shown). The canonical patterns are retrieved for each season, as presented in Wheeler and Hendon (2004) (i.e. their Figures 8 and 9).

3. Statistical-dynamical hybrid models

The hybrid models are developed based on the CFS forecast in the PC phase space rather than the physical space, thereby enabling the degree of freedom for field variables to be reduced and the computational burden drastically eased. The most informative first two PCs are used to construct the models. The original daily PCs are converted to pentad points for simplicity. To achieve the consistent evaluation of the MJO forecast skill in the dynamical and empirical models, the first 13-years of the sample data are used for the development of statistical-dynamical models and the last 10 years of data are used as validation or independent data.

The first statistical-dynamical hybrid scheme is a lagged multiple linear regression model (which is referred to as HYBRID1), where the predictors are the previous values of the first two dominant PCs, in addition to the latest observed first two PCs. Predictands are the PCs in the future. This model takes the form of

$$PC_k(t+h) = \sum_{j=0}^{J} \sum_{i=1}^{I=2} C_{kij}(h) \mathrm{PC}_{i,j}(t) + \varepsilon_{t+h} \qquad (1)$$

where PC_k are the predicted PCs and $\mathrm{PC}_{i,j}$ represent the CFS model-predicted PCs with lead time j. The latest observed PCs are always included in this model and are denoted as $\mathrm{PC}_{i,0}$ (i.e. when $j = 0$). The regression coefficients of the kth PC, $C_{kij}(h)$, which are determined by least squares estimation using the observed PCs and CFS PCs during the training period, are a function of each forecast horizon h, CFS ith PC, and lead time j. ε_{t+h} are random errors that are assumed to be normally distributed. Since the PCs are orthogonal to each other, any colinearity in the predictors can be avoided, thereby ensuring the feasibility of the computational derivation of the regression coefficients. By fitting the CFS model output to the observed information of the MJO, any systematically behaving model errors are corrected. The

DOI: 10.1002/joc

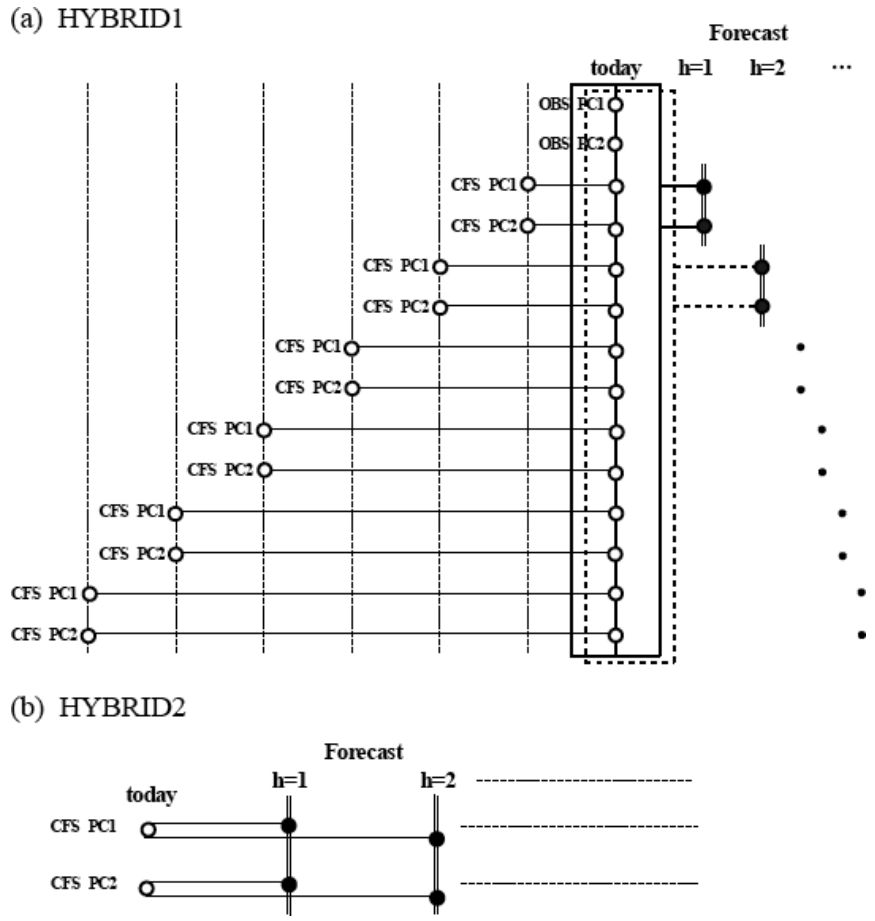

Figure 2. Schematic of (a) HYBRID1 and (b) HYBRID2 model structures. The HYBRID1 model consists of 2 predictors from two leading PCs from observations and 12 predictors from two leading PCs of CFS forecasts with 6 different lead times. Whereas the HYBRID1 is a lagged multiple linear regression model, the HYBRID2 model has one-to-one correspondence between the CFS forecasted PCs and the final, empirically predicted PCs for the same forecast times.

schematic structure of the prediction model is shown in Figure 2(a), where one pair of observed PCs and six pairs of PCs with different lead times used for prediction are shown inside the solid or dotted box. This example shows the determination of the future one or two pentad values of PCs. To select the optimal number of predictors, the predictive skills of the hybrid model for different CFS forecast lead times are computed for the PC1 and PC2 phases using the training data. The results for the correlation skills are shown in Figure 3. It is evident that the forecast skill gradually increases with increasing number of the predictors used. However, the use of more than 6 pentad leads (denoted as a thick solid line in Figure 3) does not significantly improve the correlation skill for the two PCs. Therefore, six pentad leads ($J = 6$) are chosen here. The inclusion of more PCs only slightly changes its skill (not shown).

The second statistical-dynamical forecast model (referred to as HYBRID2) is constructed to fit the CFS PC time series to the observed PC time series at the corresponding forecast time. This scheme can be written as:

$$PC_k(t+h) = \sum_{i=1}^{I=2} C_{ki}(h)\mathrm{PC}_i^{\mathrm{CFS}}(t+h) + \varepsilon_{t+h} \qquad (2)$$

where $\mathrm{PC}_i^{\mathrm{CFS}}$ represent the CFS forecast PCs for ith mode. The regression coefficients $C_{ki}(h)$ are determined by least squares estimation using the first two CFS PCs at forecast time h and the observed PCs at the corresponding validation time. Again, ε_{t+1} are random components. Therefore, future h pentad values are estimated by multiplying the $C_{ki}(h)$ derived from the training data and the predicted PCs from the CFS model (Figure 2(b)). Again, the use of more than two PCs in the model only slightly changes its skill (not shown).

Whereas only the available forecast data are used for the calculation of CFS forecast skill, the hybrid models are constructed based on the filled data in order to facilitate the estimation of the regression coefficient.

4. Results

Figure 4 shows the correlation and root mean square (RMS) error skills for PC1 and PC2 during the validation period (1995–2004) for the coupled CFS and hybrid forecasts. Persistence forecast skills are denoted as dotted lines. The threshold correlation for skillful forecast is 0.5 (horizontal lines). It is seen that the skillful CFS forecast is out to 2 and 3 pentads for PC1 and PC2, respectively,

DOI: 10.1002/joc

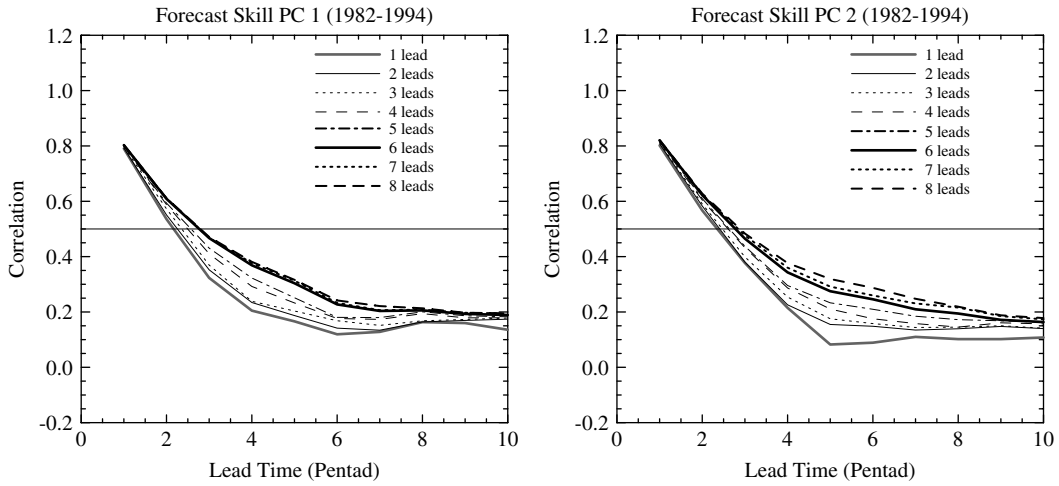

Figure 3. Sensitivity test for the HYBRID1 forecast scheme. The correlation skills for the different CFS forecast leads employed are shown for PC1 (left panel) and PC2 (right panel). The latest observed PCs are always included in the scheme. The correlation is calculated with the 13-year (1982–1994) training data.

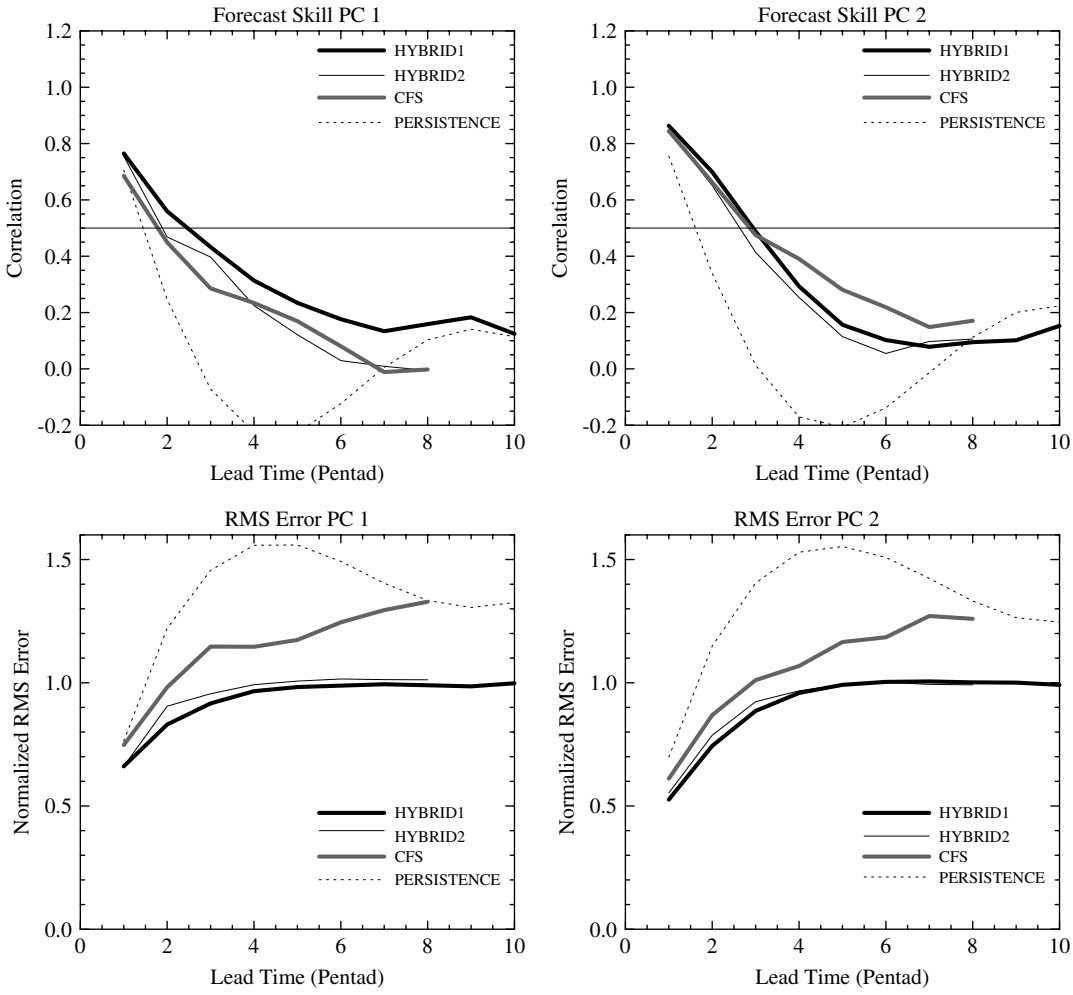

Figure 4. Correlation skill (upper panels) and normalized RMS error (lower panels) as a function of forecast lead time (in units of pentad) for PC1 (left panels) and PC2 (right panels). The calculation is based on the 10-year (1995–2004) validation data.

which is much greater than the persistence forecast skill. This difference between the PC1 and PC2 phases is primarily attributed to a propagation barrier or predictability barrier present in the NCEP atmospheric and coupled models. The previous dynamical extended-range forecast (DERF) run with GFS model demonstrated the existence of the predictability barrier over the Maritime Continent and western Pacific (Seo *et al*., 2005). This kind of the

DOI: 10.1002/joc

model deficiency was also found in a recent analysis on the CFS long-term simulation (Seo *et al*., 2007). This property in the operational coupled model is investigated in more detail in a separate paper (Seo *et al*., 2008).

The HYBRID2 forecast presents only slightly improved correlation skill compared to the CFS forecast for PC1, whereas the CFS skill is better than HYBRID2 for PC2. On the other hand, the HYBRID1 forecast skill is considerably enhanced compared to the CFS forecast, especially for the PC1 phase. The correlation skill is increased by ∼20–50%. This statistical-dynamical scheme based on the multiple lagged regression method is consistently better than the HYBRID2 forecast for all lead times. In addition to the correlation skill evaluation, the forecast amplitude error also needs to be assessed to provide the overall picture of forecast performance (Hoffman *et al*., 1995). This has been estimated in terms of the normalized RMS error. The normalization is performed using long-term persistence forecasts (see also LH00). In the figure, both hybrid schemes clearly exhibit a significant correction in RMS error relative to the CFS forecast. The HYBRID1 RMS error, which is less than that of HYBRID2, is reduced by ∼15–20%. The normalized RMS error increases with increasing forecast lead time but tends to reach saturation after 4–5 pentads, so that since the hybrid models consider the MJO as a damped oscillatory system, their RMS errors tend to approach a value of 1. These two estimates of forecast skill demonstrate the superiority of the HYBRID1 forecast compared to the CFS and HYBRID2 forecasts. HYBRID1 is considered superior to HYBRID2 because its forecast skill stems from both the autocorrelation of each PC and the lagged cross-correlation between the two PCs, while the latter does not utilize useful lagged information.

Even if RMS error is improved for PC2 using the hybrid models, the correlation skill is not improved since the CFS model produces an eastward propagation within the Indian Ocean, as appeared in the observations. Therefore, when the initial MJO is located in the central Indian Ocean, the MJO phase, but not its magnitude, is relatively well forecasted by the CFS model. Once the forecasted MJO propagates into the Maritime Continent region, it becomes stalled due to the presence of the propagation barrier. Unfortunately, this model deficiency is not corrected by the hybrid models, as they produce a damped forecast field. This is one of the limitations of the statistical correction methods.

Some seasonal differences appear in the forecast skills for the CFS and hybrid model forecasts. Figure 5 shows the CFS and HYBRID1 forecast skills as a function of forecast lead time during the winter and summer seasons for the two phases. The HYBRID2 results are not shown in the figure because its correlation skill is less than HYBRID1 for all cases. First, as expected, the CFS forecast skill in the winter season is larger than the summer season for all cases. The PC2 phase has a higher forecast skill than does the PC1 phase, and this difference is most pronounced in the summer season.

The figure also shows that CFS forecast skill for PC1 in the summer season is as small as the persistence forecast skill. The forecast skills show little variation between the winter and summer seasons for the PC2 phase, which is attributed to the existence of a strong MJO convection signal over the Indian Ocean in both seasons. In contrast, the summertime MJO convection anomalies are less pronounced than the wintertime counterpart over the Maritime Continent and western Pacific (refer to Figures 7 and 8 in WH04), so the PC1 phase shows considerable differences between the winter and summer seasons. Notice that the HYBRID1 forecast for PC1 shows better forecast skill than the CFS PC1. Moreover, the HYBRID1 correction with respect to CFS is the most effective for the PC1 phase in the summer season and this improvement is gained at all lead times. Although the HYBRID1 forecast skill of winter and summer seasons for the PC2 phase does not show any noticeable improvement compared to CFS, the amplitude RMS error is moderately improved (not shown).

Figure 6 shows the correlation skill as a function of forecast lead time for ENSO states during the winter season (November through April). To include more extreme ENSO cases, the skill is calculated for the whole CFS data period starting from 1982 to 2004. El Niño and La Niña years are selected according to the criteria developed by NOAA utilizing the SST anomaly in the Nino3.4 region. An El Niño condition occurs when the three-month running mean Nino3.4 index is at least 0.5 °C for at least five consecutive months; conversely, La Niña occurs when this index is −0.5 °C or less for five consecutive months. The El Niño years in the study period are 1982, 1987, 1991, 1994, 1997, 2002 and 2004 and the La Niña years are 1985, 1988, 1995, 1998, 1999 and 2000. The slight changes of the selected years for each case produce only negligible differences. It is seen that during the ENSO winter season, the forecast skill only extends out to ∼2 pentads for both PC1 and PC2 cases. However, the skill in the La Niña years exceeds 3 pentads, which is noticeably greater than the El Niño case. This may be related to the previous findings indicating the presence of weaker MJO activity in El Niño conditions and stronger activity in La Niña conditions. Since the observed MJO activity is stronger in the La Niña years, the HYBRID1 correction is much more effective. The RMS errors are reduced by ∼15–30% (not shown). The forecast skill during the ENSO summer seasons is also calculated (not shown). It is found that the CFS forecast skill for PC1 during the El Niño summer is the worst among all cases and even HYBRID1 has a forecast skill of less than 3 pentads. The improvement rate achieved by HYBRID1 during the summer season is only about half of the improvement for the ENSO winter cases.

Finally, an example of CFS and HYBRID1 forecasts of OLR anomalies is presented, along with the corresponding observed fields, in Figure 7. The forecast initial date is 1 January, 1996. The observed MJO event illustrates the development of an enhanced convection

DOI: 10.1002/joc

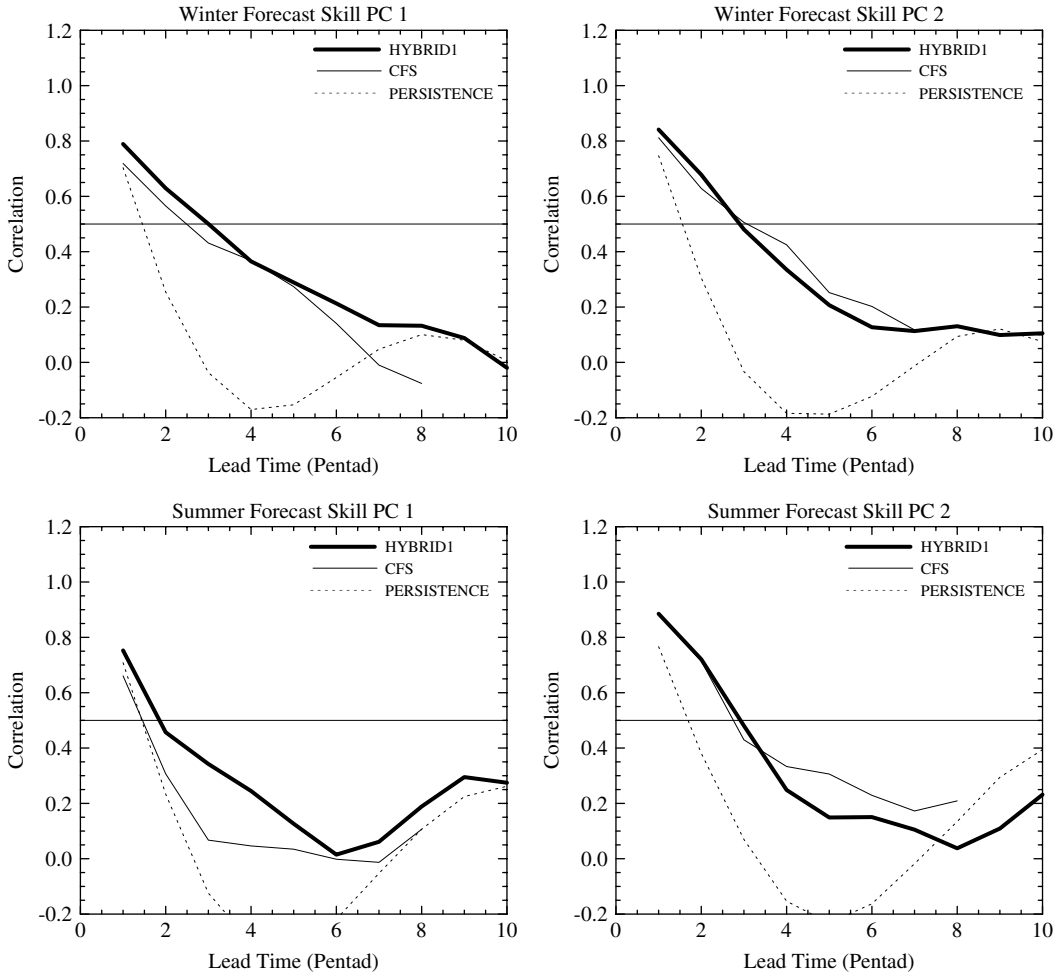

Figure 5. Correlation skill in the winter (upper panels) and summer (lower panels) seasons for PC1 (left panels) and PC2 (right panels). The calculation is based on the 10-year (1995–2004) validation data.

over the Indian Ocean during the first three pentads and its subsequent eastward propagation across the Maritime Continent. Initially, the suppressed convection is dominant over the broad region from the East Indian Ocean to the western Pacific. CFS cannot properly initiate the MJO convection signal and its growth over the Indian Ocean. The eastward propagation is also poorly observed. By contrast, the HYBRID1 forecast shows similar characteristics to those identified in the observations; a suppressed convection over the Maritime Continent propagates eastward and decays near the dateline, while an enhanced convection, once developed over the Indian Ocean, propagates to the east. The phase and amplitude of the major MJO signals are reasonably well forecasted. Only a suppressed convection over the Indian Ocean in pentads 4 and 5 is not represented. In this example, the phase, amplitude, and propagation are effectively adjusted by the statistical-dynamical hybrid method.

5. Summary and Discussion

This work examines the performance of the MJO forecast in the NCEP's operational coupled model (CFS). Using the projection of ENSO-removed variables onto the principal patterns of the MJO convection and upper- and lower-level circulations, the MJO-related signals in the dynamical model forecasts are extracted. It is found that the coupled model demonstrates a useful skill out to 2 and 3 pentads when the initial MJO convection is located over the Maritime Continent and the Indian Ocean, respectively. Based on this dynamical model forecast, statistical-dynamical hybrid models are developed for improved predictability. The first hybrid model (HYBRID1) is a lagged multiple linear regression scheme, where the previous values of the first two leading PCs from the coupled model are used as predictors. The other hybrid model (HYBRID2) is constructed to fit the predicted PC time series from the coupled model to the observed PCs at each lead time using 13 years of training data fields.

HYBRID2 does not improve the forecast skill persistently, whereas in HYBRID1, which utilizes lagged correlation information, the resulting correlation coefficient and RMS skills show a considerable, robust enhancement. In HYBRID1, the skill improvement ranges from 15 to 50% with respect to the CFS forecast and the improvement in the correlation skill is larger than the RMS error correction.

DOI: 10.1002/joc

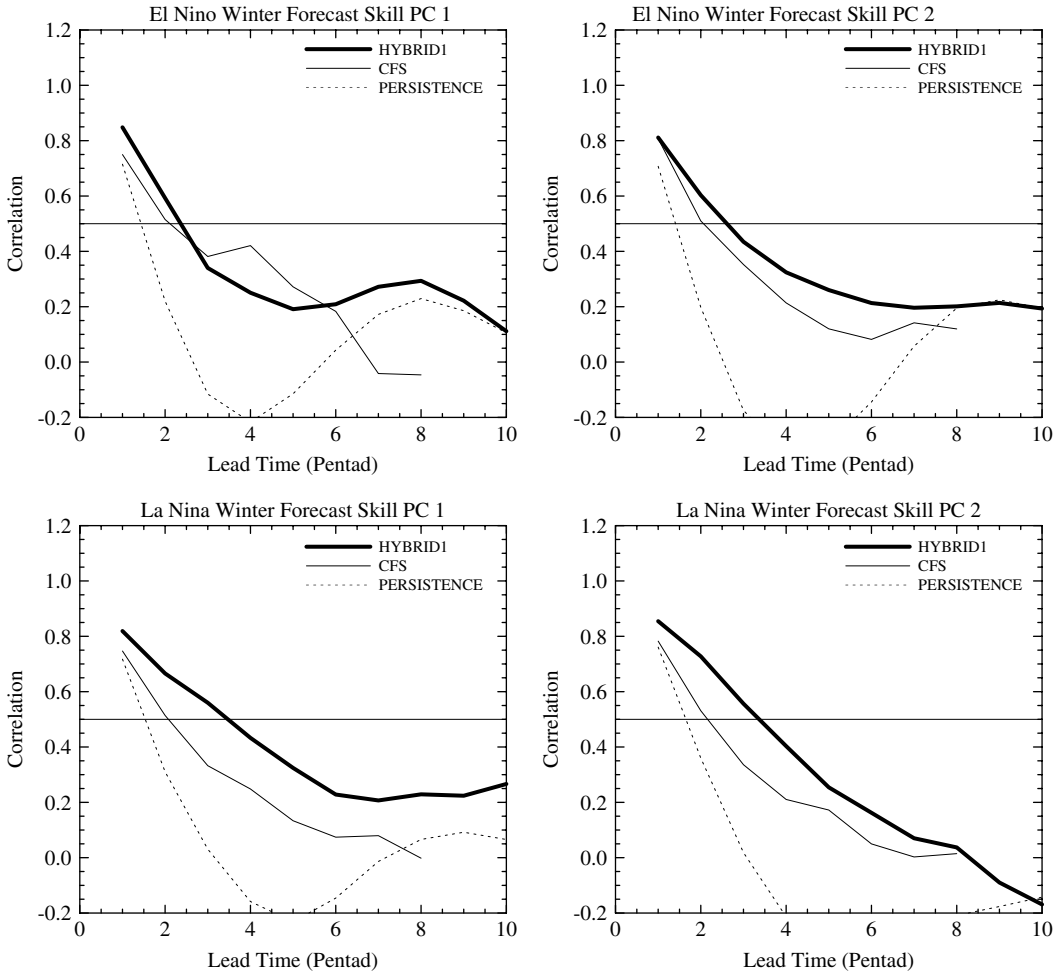

Figure 6. Correlation skill in the winter season during El Niño (upper panels) and La Niña (lower panels) years for PC1 (left panels) and PC2 (right panels). The calculation is based on the 23-year (1982–2004) validation data.

The variation in forecast skill according to the season is also examined. As in the previous findings (e.g. Jones *et al*., 2000; Seo *et al*., 2005), the predictive skill is higher during the northern winter than during the northern summer in CFS and HYBRID1. Furthermore, when the MJO convection is located initially over the Maritime Continent during the northern summer, the CFS forecast skill is as small as the persistence forecast, but a superior correction is achieved by adjustment of the HYBRID1 statistical method. The HYBRID1 skill is enhanced by ∼30% compared to the CFS forecast during ENSO winters and the skill improvement in La Niña years is noticeably greater than in El Niño years.

The improvement of the MJO forecast skill gained by the statistical-dynamical hybrid model depends on the extent to which the CFS model behaves in a persistent manner for the prediction of the MJO convection and circulation anomalies. In other words, as much as the CFS model predicts the MJO's amplitude and propagation characteristics in a constant way (i.e. either eastward, westward or stationary), the hybrid model produces a much better prediction. Another difficulty is associated with the die-out of the intraseasonal signal in the CFS model forecast with increasing lead time as shown in the recent study by Seo *et al*. (2008). When the MJO signals from a dynamical forecast model decrease with increasing forecast time, the regression is not very efficient in nature. Nevertheless, since the MJO temporal scale bridges the gap between synoptic weather forecasting and seasonal forecasting, the information on the MJO predictability in the current operational dynamical model and in empirical forecast models is important and the improved forecasting of the tropical intraseasonal signal should provide better predictions of the MJO-related weather and climate in all global regions, including midlatitude circulation and precipitation anomalies (e.g. Ferranti *et al*., 1990; Higgins and Mo, 1997; Higgins *et al*., 2000; Jeong *et al*., 2008) and the development of tropical cyclones in the Pacific and Atlantic oceans (e.g. Maloney and Hartmann, 2000; Higgins and Shi, 2001; Kim *et al*., 2008).

Acknowledgements

The author thanks Drs Matt Wheeler and J. -S. Kug for their valuable comments and suggestions. This work was funded by the Korea Meteorological Administration Research and Development Program under Grant CATER 2007-4208. The author would like to acknowledge the

DOI: 10.1002/joc

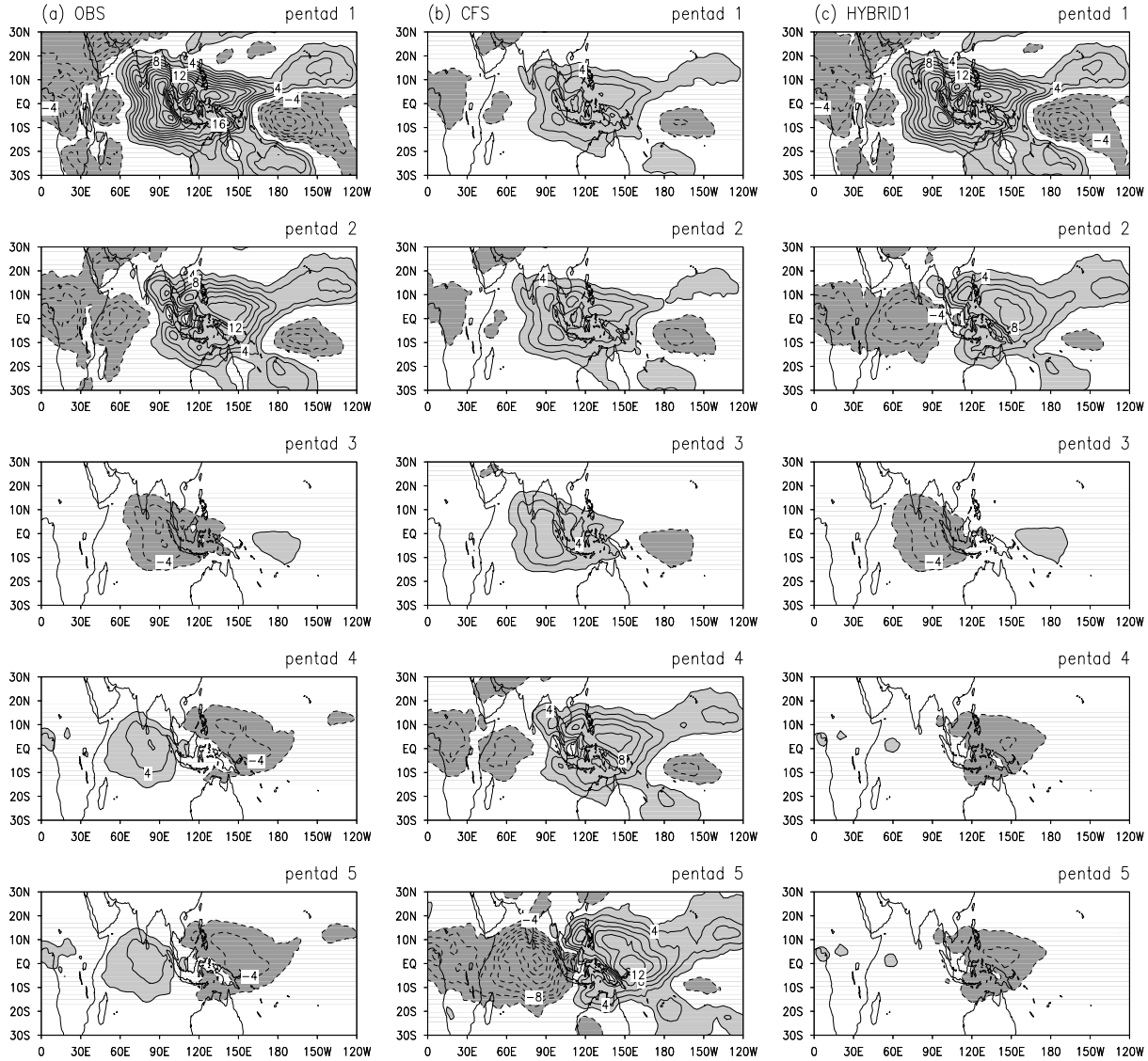

Figure 7. An example of CFS and HYBRID1 forecasts of OLR anomalies. The corresponding validation fields are also plotted. The forecast initial date is 1 January, 1996. (a) Observations, (b) CFS forecast, and (c) HYBRID1 forecast. Contour intervals are 2 W m^{-2}.

support from KISTI (Korea Institute of Science and Technology Information).

References

Ferranti L, Palmer TN, Molteni F, Klinker E. 1990. Tropical-extratropical interaction associated with the 30–60 day oscillation and its impact on medium and extended range prediction. *Journal of the Atmospheric Sciences* **47**: 2177–2199.

Hendon HH. 2000. Impact of air-sea coupling on the Madden-Julian Oscillation in a general circulation model. *Journal of the Atmospheric Sciences* **57**: 3939–3952.

Higgins RW, Mo KC. 1997. Persistent North Pacific circulation anomalies and the tropical intraseasonal oscillation. *Journal of Climate* **10**: 224–244.

Higgins RW, Schemm JKE, Shi W, Leetmaa A. 2000. Extreme precipitation events in the Western United State related to tropical forcing. *Journal of Climate* **13**: 793–820.

Higgins RW, Shi W. 2001. Intercomparison of the principal modes of interannual and intraseasonal variability of the North American monsoon system. *Journal of Climate* **14**: 403–417.

Hoffman RN, Liu Z, Louis JF, Grassotti C. 1995. Distortion representation of forecast errors. *Monthly Weather Review* **123**: 2758–2770.

Jeong JH, Kim BM, Ho CH, Noh YH. 2008. Systematic variation in wintertime precipitation in East Asia by MJO-induced extratropical vertical motion. *Journal of Climate* **21**: 788–801.

Jones C, de Carvalho LMV. 2002. Active and break phases in the South American Monsoon System. *Journal of Climate* **15**: 905–914.

Jones C, Waliser DE, Schemm JKE, Lau KM. 2000. Prediction skill of the Madden-Julian oscillation in dynamical extended range forecasts. *Climate Dynamics* **16**: 273–289.

Kanamitsu M, Ebisuzaki W, Woollen J, Yang SK, Hnilo JJ, Fiorino M, Potter GL. 2002. NCEP-DOE AMIP-II reanalysis (R-2). *Bulletin of the American Meteorological Society* **83**: 1631–1643.

Kessler W, Kleeman R. 2000. Rectification of the Madden-Julian oscillation into the ENSO cycle. *Journal of Climate* **13**: 3560–3575.

Kim JH, Ho CH, Kim HS, Sui CH, Park SK. 2008. Systematic variation of summertime tropical cyclone activity in the western North Pacific in relation to the Madden-Julian oscillation. *Journal of Climate* **21**: 1171–1191.

Lau KM, Chan PH. 1986. Aspects of the 40–50 day oscillation during the northern summer as inferred from the outgoing longwave radiation. *Monthly Weather Review* **114**: 1354–1367.

Liebmann B, Smith CA. 1996. Description of a complete (interpolated) outgoing longwave radiation dataset. *Bulletin of the American Meteorological Society* **77**: 1275–1277.

Lo F, Hendon HH. 2000. Empirical extended-range prediction of the Madden-Julian oscillation. *Monthly Weather Review* **128**: 2528–2543.

DOI: 10.1002/joc

Madden RA, Julian PR. 1971. Detection of a 40–50 day oscillation in the zonal wind in the tropical Pacific. *Journal of the Atmospheric Sciences* **28**: 702–708.

Madden RA, Julian PR. 1972. Description of a 40–50 day oscillation in the zonal wind in the tropical Pacific. *Journal of the Atmospheric Sciences* **29**: 1109–1123.

Maloney ED, Hartmann DL. 2000. Modulation of eastern north Pacific hurricanes by Madden-Julian oscillation. *Journal of Climate* **13**: 1451–1460.

McPhaden MJ. 1999. Genesis and evolution of the 1997–1998 El Niño. *Science* **283**: 950–954.

McPhaden MJ. 2004. Evolution of the 2002/03 El Niño. *Bulletin of the American Meteorological Society* **85**: 677–695.

Mo KC. 2000. Intraseasonal modulation of summer precipitation over North America. *Monthly Weather Review* **128**: 1490–1505.

Pacanowski RC, Griffies SM. 1998. *MOM 3.0 Manual*. NOAA/ Geophysical Fluid Dynamics Laboratory: Princeton, NJ.

Reynolds RW, Rayner NA, Smith TM, Stokes DC, Wang W. 2002. An improved in situ and satellite SST analysis for climate. *Journal of Climate* **15**: 1609–1625.

Saha S, Nadiga S, Thiaw C, Wang J, Wang W, Zhang Q, Van den Dool HM, Pan HL, Moorthi S, Behringer D, Stokes D, Pena M, Lord S, White G, Ebisuzaki W, Peng P, Xie P. 2006. The NCEP climate forecast system. *Journal of Climate* **19**: 3483–3517.

Seo KH, Schemm JKE, Jones C, Moorthi S. 2005. Forecast skill of the tropical intraseasonal oscillation in the NCEP GFS dynamical extended range forecasts. *Climate Dynamics* **25**: 265–284.

Seo KH, Schemm JKE, Wang W, Kumar A. 2007. The boreal summer intraseasonal oscillation simulated in the NCEP Climate Forecast System (CFS): The effect of sea surface temperature. *Monthly Weather Review* **135**: 1807–1827.

Seo KH, Wang W, Gottschalck J, Zhang Q, Schemm JKE, Higgins WR, Kumar A. 2008. Evaluation of MJO forecast skill from several statistical and dynamical forecast models. *Journal of Climate* DOI: 10.1175/2008JCLI2421.1.

Seo KH, Xue Y. 2005. MJO-related oceanic Kelvin waves and the ENSO cycle: A study with the NCEP Global Ocean Data Assimilation. *Geophysical Research Letter* **32**: L07712, DOI: 10.1029/2005GL022511.

Trenberth KE, Branstator GW, Karoly D, Kumar A, Lau NC, Ropelewski C. 1998. Progress during TOGA in understanding and modeling global teleconnections associated with tropical sea surface temperatures. *Journal of Geophysical Research* **103**: 14291–14324.

Wang W, Saha S, Pan HL, Nadiga S, White G. 2005. Simulation of ENSO in the new NCEP Coupled Forecast System Model (CFS). *Monthly Weather Review* **133**: 1574–1593.

Waliser DE, Lau KM, Stern W, Jones C. 2003. Potential predictability of the Madden-Julian Oscillation. *Bulletin of the American Meteorological Society* **84**: 33–50.

Wheeler M, Hendon HH. 2004. An all-season real-time multivariate MJO index: Development of an index for monitoring and prediction. *Monthly Weather Review* **132**: 1917–1932.

Zhang C, Gottschalck J. 2002. SST anomalies of ENSO and the Madden-Julian Oscillation in the equatorial Pacific. *Journal of Climate* **15**: 2429–2445.